

Manifesting pseudo-spin polarization on the edge of graphene via field emission image

Jingkun Chen, Zhibing Li¹, Weiliang Wang

State Key Laboratory of Optoelectronic Materials and Technologies, School of Physics and Engineering, Sun Yat-sen University, Guangzhou, P.R. China 510275

Abstract

Field emission wave function from graphene in magnetic field is obtained. The emission image reveals structure of the Landau levels and depends on the phase difference between two sub-lattices. The emission pattern is sensitive to the edge potential shift that can be controlled via a gate voltage on the edge.

Low energy behavior of graphene can be described by two-dimensional chiral fermions with pseudo-spin associating to the bi-lattice structure of graphene [1]. The degree of freedoms of pseudo-spin has been observed indirectly in a number of experiments [2-4]. A recent beautiful experiment has shown the chirality and Berry phases of graphene via photoemission [5]. The present letter investigates a possibility of extracting pseudo-spin polarization via electric field assisted electron emission from graphene under a perpendicular magnetic field. We find that the emission pattern can be manipulated by a gate voltage on the edge.

Several groups have demonstrated that graphene does show promising field electron emission (FE) properties such as a low emission threshold field and large emission current density [6-14]. Theoretical studies suggested that the characteristic current-field relation of a 2D emitter is different from the Fowler-Nordheim law for conventional emitters [15-17]. Coherent cold field emission (CCFE) patterns have been observed experimentally [6]. A dragonfly-like pattern of CCFE was predicted theoretically for an ideal graphene field emitter in the absent of magnetic field[18]. It implies that it is possible to extract information of quantum states of the emitter via CCFE. A profound effect of magnetic field on two-dimensional electron gases is the quantum Hall effect (QHE) that has been realized in graphene [19, 20] and can be observed even at room temperature [19-21]. It has been known that the QHE of graphene is substantially different from that of non-relativistic electron gases [22]. Graphene QHE has the zero-energy Landau level which is absent in the non-relativistic QHE. In the present text, Landau levels in the vicinity of the Fermi level play important role. In bulk graphene all states of a given Landau level are degenerate. The edge effect lifts the degeneracy such that each Landau level splits into two bands [23, 24]. The splitting becomes significant in magnetic fields of order of Tesla. Therefore CCFE from various edge states may be distinguished in strong enough magnetic fields.

The model is an individual graphene mounted on a planar cathode vertically, with the free edge terminated by hydrogen atoms. Let the graphene lie on the x - y plane in the regime of $-\hbar < x < 0$, with the emission edge along the y axis. A uniform macroscopic electric field F_0 in the negative x direction is applied on the graphene via an anode that is far away from the graphene presumably. In a proper approximation [18], the potential energy barrier for the p -th eigenstate has

¹Corresponding author: stslzb@mail.sysu.edu.cn

the form $V(\vec{r}) = W_p - eF_0\sqrt{\hbar(x + \sqrt{x^2 + z^2})}$. The zero-field effective barrier height reads

$$W_p = W_0 - E_p + \frac{(\hbar k)^2}{2m} \quad (1)$$

Where $W_0=4.32\text{eV}$ is the work function [25], E_p the eigenenergy related to the Fermi level of neutral graphene (referred to as intrinsic Fermi level). The last term is the transversal kinetic energy with k the y -directional wave number. The zigzag and armchair edges terminated by hydrogen atoms are two edges often discussed in the literatures. However it was argued that the zigzag edge terminated with hydrogen atoms has ignorable contribution to FE because the relevant states have large transversal kinetic energies [16]. Therefore we will concentrate on the armchair edge.

Graphene CCFE will be treated as coherent decay of edge atomic orbitals (EAOs). Because the relevant electronic properties of graphene can be attributed to the π -orbitals of graphene, we may assume that the EAOs have the form of the π -orbitals. The smooth matching condition determines the characteristic length $1/\tau_p = \hbar/\sqrt{2mW_p}$ of the EAO for a given p -state. The path-decomposition method provides a bridge that connects the emission wave function and the collective quantum state of the emitter coherently. The merit of this approach is that the exact core potential which is usually un-known is not inquired [18].

Because most electric field in graphene is screened, one can first find the eigenstates of graphene in the absent of electric field. Then the residual macroscopic electric potential in graphene may be accounted via the level bending. It is known that the energy states near the intrinsic Fermi level are located in the Dirac cones where the dispersion relation is linear. There are two independent pairs of Dirac cones with vertexes (Dirac points) $\mathbf{K}_\pm = (\pm K, 0)$ with $K = \frac{4\pi}{3\sqrt{3}a}$ and the bond length $a = 0.142$ nm. In a magnetic field pointing to the z direction, an eigenstate of a given k is localized in the x direction, if Landau gauge $\mathbf{A} = (0, Bx, 0)$ is chosen. Without losing generality, $B > 0$ will be assumed. A x -directional localized amplitude is described by a pair of Weyl spinors [23], $\Psi_p^{(L)} = (\psi_{p,A}^{(L)}(x), \psi_{p,B}^{(L)}(x))^T$ and $\Psi_p^{(R)} = (\psi_{p,B}^{(R)}(x), \psi_{p,A}^{(R)}(x))^T$, where the superscript $L(R)$ is referred to the left-handed (right-handed) spinor associated with $\mathbf{K}_- (\mathbf{K}_+)$ Dirac cone, and the subscript A (B) is referred to the pseudo-spin associated with the A(B)-sublattice. The real spin degree of freedoms is not shown here because the Zeeman Effect has been neglected. The eigenenergy related to the intrinsic Fermi level can be written as $E_p = s\sqrt{\lambda_p}\varepsilon_0$ where $s = \pm 1$ is the signature of the energy band, while $\varepsilon_0 = \frac{\sqrt{2}\hbar v_F}{l_B}$ is the energy unit with $v_F \sim c/330$ the Fermi velocity and $l_B = \sqrt{\frac{\hbar}{eB}}$ a characteristic length associated with B . The dimensionless number λ_p is to be determined by the boundary conditions.

Due to the symmetry, the y -directional wave number k is conserved. In the graphene regime ($x < 0$), the effective potential for a component of the Weyl spinors with a given k is a parabolic potential minimized at $\tilde{x}_0 = -\xi_0 = -kl_B$. For large positive k , i.e., large negative \tilde{x}_0 , the edge effect is negligible. Thus λ_p converges to a non-negative integer n ($n = 0, 1, 2, \dots$), with which the Landau levels are labeled. The components of the Weyl spinors can be written in the parabolic cylinder function D_λ

$$\psi_{p,A}^{(R)}(x) = e^{-i\frac{s\xi}{4}} N_p D_{\lambda_p}(\sqrt{2}\xi) \quad (2)$$

$$\psi_{p,B}^{(R)}(x) = i s e^{-i\phi_p - i\frac{s\xi}{4}} \sqrt{\lambda_p} N_p D_{\lambda_p-1}(\sqrt{2}\xi) \quad (3)$$

$$\psi_{p,A}^{(L)}(x) = \eta e^{-i\frac{s\xi}{4}} \sqrt{\lambda_p} N_p D_{\lambda_p-1}(\sqrt{2}\xi) \quad (4)$$

$$\psi_{p,B}^{(L)}(x) = i \eta s e^{-i\phi_p - i\frac{s\xi}{4}} N_p D_{\lambda_p}(\sqrt{2}\xi) \quad (5)$$

Where $\xi = \frac{x}{l_B} + kl_B$, $\eta = \pm 1$, and ϕ_p is the phase difference between two sub-lattices. The boundary conditions for the armchair edge are $\sigma_1 \psi_{p,\alpha}^{(R)}(0) + \psi_{p,\alpha}^{(L)}(0) = 0$ for $\alpha = A$ and B. Substitution of (2-5) in the boundary conditions yields $D_{\lambda_p}(\sqrt{2}\xi_0) = -\eta \sqrt{\lambda_p} D_{\lambda_p-1}(\sqrt{2}\xi_0)$, from which one can determine λ_p . The normalization factor $N_p = (4l_B \int_{-\infty}^{\xi_0} d\xi \mathcal{D}_{\lambda_p}^2)^{-\frac{1}{2}}$. Note that the Hamiltonian conserves the time-Y parity that is defined as the combination transform of time reverse and the y -directional reflection. With the constant phase $e^{-i\frac{s\xi}{4}}$ introduced in the Weyl spinors, the time-Y parity is equal to η . Therefore an eigenstate is specified by four quantum numbers (n, s, k, η) which are denoted by p for brevity. The $n = 0$ Landau level is special for the massless Weyl spinor, that has only $\eta = -1$ states.

Tunneling through the two-dimensional barrier $V(\vec{r})$ may be solved by a conformal transformation of the x - z plane that maps the projection of the cathode and graphene into a straight line. In the transformed plane, the outer turning point of the potential energy barrier is $\tilde{x}_1 = \frac{W_p}{eF_0}$. The emission wave function has been obtained by the path-decomposition method [18] that in large distance has the asymptotic form

$$\varphi_p(\vec{r}) \sim \tilde{C}_p \left(\frac{\tilde{x}_1}{x}\right)^{1/4} \chi(z) S_p^{\frac{s}{4}} e^{-\frac{\hbar_0}{2} S_p - \frac{1}{4}(2 - S_p + \sqrt{S_p^2 + 4})} \frac{e^{iky}}{\sqrt{L}} \quad (6)$$

Where \tilde{C}_p is the amplitude of the tight-binding model on the edge carbons, L is the length of the

edge. The dimensionless factor $S_p = \frac{4\tau_p \bar{x}_1^2}{9h}$ and the constant $b_0 = 1 + \frac{4}{5\sqrt{3}}$. The z -directional distribution is given by the square-normalized amplitude $\chi_p(z) = \frac{c_1 \mu_p^{3/4}}{\sqrt{x}} \frac{z}{x} e^{-\frac{\mu_p}{2} (\frac{z}{x})^2}$ with $\mu_p = \frac{c_2 k_a^2 h}{\tau_p}$ and $k_a = \frac{1}{h} \sqrt{2meF_0 x}$. Two numerical constants $c_1 \sim 1.2$ and $c_2 \sim 0.45$ have been introduced for the brevity.

Let Δ be the edge energy shift with respect to the intrinsic Fermi level. A finite Δ as a result of band-bending may be created by the field penetration [16, 18]. It may also be controlled by a gate voltage on the edge. With the wave function (6) it is straight forward to calculate the emission current density on the screen. Let both screen and anode locate at the same plane in distance x_a from the emitter. We obtain the electric current density on the screen

$$j(y, z) = \sum_p \frac{c_0 e \tau_p}{2\pi a^2 t_a} \frac{|\tilde{C}_p|^2 |\chi(z)|^2}{e^{(E_p - \Delta)/(k_B T)} + 1} S_p^{\frac{5}{2}} e^{-b_0 S_p - \frac{1}{2}(2 - S_p + \sqrt{S_p^2 + 4})} \Bigg|_{k = \frac{my}{\hbar x_a}} \quad (7)$$

Where T is the temperature of graphene, the numerical constant $c_0 \approx 0.1$. In the near axis regime and for large x_a , the k wave will reach the screen at position $y = \frac{\hbar k}{m} t_a$ with $t_a = \sqrt{\frac{2mx_a}{eF_0}}$ the flying time. Using the spinor amplitudes given in (2-6), the probability of electron in the p -state to appear in the edge carbon orbitals turns out to be

$$|\tilde{C}_p|^2 = \frac{3^{5/2} a^2}{2} |N_p D_{\lambda_p}(\sqrt{2}\xi_0)|^2 (1 - \eta s \sin \phi_p) \quad (8)$$

The phase difference between two sub-lattices may be written as $\phi_p = ka + \phi_0$ with ϕ_0 a constant phase shift. The present model considered only the nearest neighbor interaction hence it is degenerate on ϕ_0 . In principle ϕ_0 would depend on the state preparing process. It would be changed by proper interactions. For instance, the spin-orbital interaction due to the next-to-nearest neighbor interaction, although that it is small in graphene, will lift the degeneracy on the phase shift in principle. The appearance of ϕ_0 represents the pseudo-spin polarization. Averaging over ϕ_0 with equal weight will get rid of the ϕ_0 -depending term in (8), leading to the un-polarized result.

In the following numerical calculations, we fix $x_a = 1$ mm, $h = L = 10$ μ m, $F_0 = 20$ V/ μ m, and $B = 15$ Tesla. Fig.1 presents a typical emission image on a screen at the room temperature, with $\Delta = 0$ and $\phi_0 = 0$. Two main peaks separated in z direction are caused by interference of two lobes of the π -orbital. Integration over z gives the y -directional line current density, as shown by the solid black curve in Fig.2 for the temperature of liquid nitrogen (77 Kelvin). Colored curves are partial current densities from individual Landau levels close to the Fermi level (see inset of the

same figure). The colors of the partial current densities follow the colors of their corresponding Landau levels. Solid and dashed curves are for positive and negative levels respectively. The structure of Landau levels exhibits as multi-peaks in the emission image.

To see the effect of the edge energy shift, the y -directional line current densities on the screen for edge energy shifts from $\Delta = -0.2\text{eV}$ to 0.2eV increasing with step 0.05eV are plotted in Fig.3 (curves from the bottom to the top) at $T = 77$ Kelvin. The image pattern obviously depends on Δ . For positive Landau levels which are bending upwards with decreasing k , the left wings of their current densities are sharply cut because the occupation numbers of these levels decrease exponentially when the levels exceed Δ . Their right wings are cut because the exponential decay of probability amplitude on the edge. On the other hand, for a negative Landau level which is bending downwards with decreasing k , sharp suppression of current distribution happens on the right wing for negative Δ . The reason for this case is two-folds: (1) the depletion of the Landau levels, (2) the exponential decay of probability amplitude on the edge. Thus, one can expect that only left wing of the current density associated with positive Landau levels is sensitive to the temperature.

The effect of the pseudo-spin polarization is shown in Fig.4 for $\Delta=0.2\text{eV}$ and $T = 77$ Kelvin. The patterns of $\phi_0 = 0$ and π almost coincide with the un-polarized pattern (black dashed) both in the middle regime and on the right wing. However the left wings of them can be clearly distinguished. The patterns of $\phi_0 = \pm \frac{\pi}{2}$ are dramatically different from the previous ones. The pattern of $\phi_0 = \frac{\pi}{2}$ has the main peak on the left and the second peak on the right. The latter is close to the origin. On the other hand, the pattern of $\phi_0 = -\frac{\pi}{2}$ has the main peak on the right, the second peak on the left, and a fat tail on the left wing. Incidentally, states with $\phi_0 = \frac{\pi}{2}$ or $\phi_0 = -\frac{\pi}{2}$ have the reflection symmetry on the x - y plane in the absent of fields. Therefore, one may build up the states with $\phi_0 = \pm \frac{\pi}{2}$ by applying electric and magnetic fields adiabatically on initial states that possessing the reflection symmetry in the absent of fields.

In summary, we obtained the analytical expression for the coherent field emission current density of the armchair edge of graphene under magnetic fields. The emission image presents two interference fringes originated from the wave function of the π -orbital. The emission pattern manifests the structure of Landau levels and can be manipulated by gate voltage on the edge. The effect of pseudo-spin polarization is discussed. When the phase different of two sub-lattices changes half $\pi/2$, the emission pattern will change dramatically. The dependence of emission pattern on the phase would enable one to read the pseudo-spin polarization by coherent field emission.

Acknowledgement: The project is supported by the Fundamental Research Funds for the Central Universities (No. 13lgy34), the National Natural Science Foundation of China (11274393 and 11104358) and the National Basic Research Program of China (2007CB935500, 2008AA03A314

and 2013CB933601).

References:

1. Semenoff, G, Physical Review Letters **53**, 2449 (1984)
2. Bostwick, A., T. Ohta, T. Seyller, K. Horn, and a.E. Rotenberg, Nature Physics **3**, 36 (2007)
3. Zhou, S.Y., G.H. Gweon, A.V. Fedorov, P.N. First, W.A. de Heer, D.H. Lee, F. Guinea, A.H. Castro Neto, and A. Lanzara, Nature Materials **6**, 770 (2007)
4. Nair, R.R., P. Blake, A.N. Grigorenko, K.S. Novoselov, T.J. Booth, T. Stauber, N.M.R. Peres, and A.K. Geim, Science **320**, 1308 (2008)
5. Liu, Y., G. Bian, T. Miller, and T.C. Chiang, Physical Review Letters **107**, 166803 (2011)
6. Hisato Yamaguchi, Katsuhisa Murakami, Goki Eda, Takeshi Fujita, Pengfei Guan, Weichao Wang, Cheng Gong, Julien Boisse, Steve Miller, Muge Acik, Kyeongjae Cho, Yves J. Chabal, Mingwei Chen, Fujio Wakaya, Mikio Takai, and M. Chhowalla, ACS Nano **5**, 4945 (2011)
7. Min Qian, Tao Feng, Hui Ding, Lifeng Lin, Haibo Li, Yiwel Chen, and Z. Sun, Nanotechnology **20**, 425702 (2009)
8. Wei Tap Zheng, Yong Min Ho, Hong Wei Tian, Mao Wen, Jun Lei Qi, and Y.A. Li, Journal of Physical Chemistry C **113**, 9164 (2009)
9. Zhong-Shuai Wu, Songfeng Pei, Wencai Ren, Daiming Tang, Libo Gao, Bilu Liu, Feng Li, Chang Liu, and H.-M. Cheng, Advanced Materials **21**, 1756 (2009)
10. Zhiming Xiao, Juncong She, Shaozhi Deng, Zikang Tang, Zhibing Li, Jianming Lu, and N. Xu, ACS Nano **4**, 6332 (2010)
11. Hojati-Talemi, P. and G.P. Simon, Carbon **49**, 2875 (2011)
12. Malesevic, A., R. Kemps, A. Vanhulsel, M.P. Chowdhury, A. Volodin, and C. Van Haesendonck, Journal of Applied Physics **104**, 084301 (2008)
13. Eda, G., H. Emrah Unalan, N. Rupesinghe, G.A.J. Amaratunga, and M. Chhowalla, Applied Physics Letters **93**, 233502 (2008)
14. Jiang, L., T. Yang, F. Liu, J. Dong, Z. Yao, C. Shen, S. Deng, N. Xu, Y. Liu, and H.-J. Gao, Advanced Materials **25**, 250 (2013)
15. Xi-Zhou Qin, Wie-Liang Wang, Ningsheng Xu, Zhibing Li, and R.G. Forbes, Proceedings of The Royal Society A **467**, 1029 (2010)
16. Wang, W., X. Qin, N. Xu, and Z. Li, Journal of Applied Physics **109**, 044304 (2011)
17. Mao, L.-F., Carbon **49**, 2709 (2011)
18. Li, Z., N. Xu, and H. Kreuzer, Physical Review B **85**, 115427 (2012)
19. Novoselov, K.S., A.K. Geim, S.V. Morozov, D. Jiang, M.I. Katsnelson, I.V. Grigorieva, S.V. Dubonos, and A.A. Firsov, Nature **438**, 197 (2005)
20. Zhang, Y., Y.-W. Tan, H.L. Stormer, and P. Kim, Nature **438**, 201 (2005)
21. K.S. Novoselov, J. Z, Y. Zhang, S.V. Morozov, H.L. Stormer, U. Zeitler, J.C. Maan, G.S. Boebinger, P. Kim, and A.K. Geim, Science **315**, 1379 (2007)
22. Peres, N., F. Guinea, and A. Castro Neto, Physical Review B **73**, 125411 (2006)
23. Brey, L. and H. Fertig, Physical Review B **73**, 195408 (2006)
24. Castro Neto, A.H., N.M.R. Peres, K.S. Novoselov, and A.K. Geim, Reviews of Modern Physics **81**, 109 (2009)
25. Wang, W. and Z. Li, Journal of Applied Physics **109**, 114308 (2011)

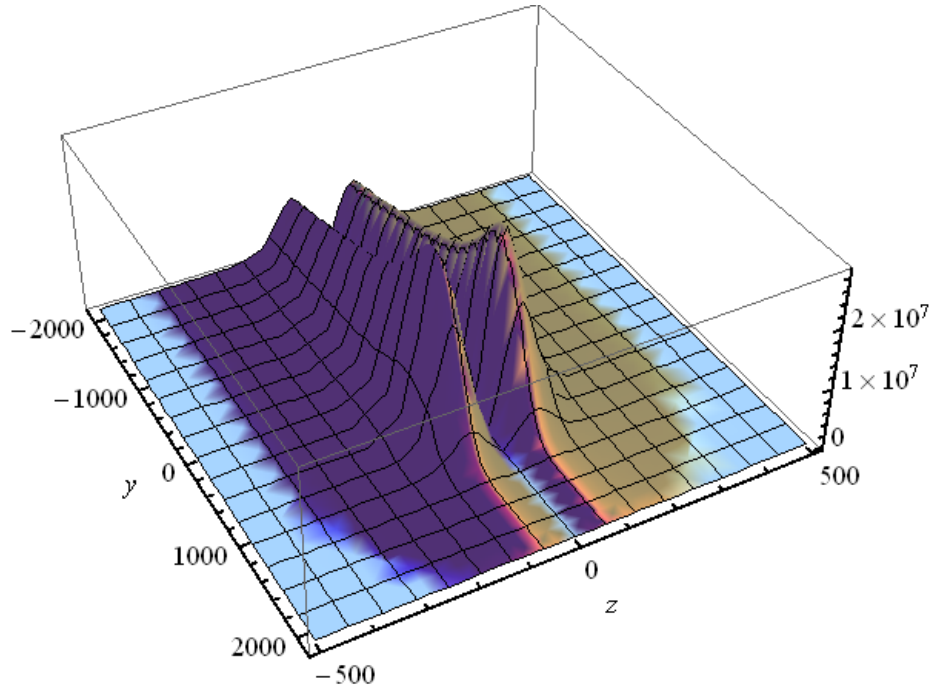


Fig.1 (color on line) The emission pattern in applied electric field of $20 \text{ V}/\mu\text{m}$ and magnetic field of 15 Tesla, at the room temperature. The vertical axis is the emission current density on the screen (mA/cm^2). The y and z coordinates are in unit of nanometer. Both the edge energy shift and the phase shift are set to zero.

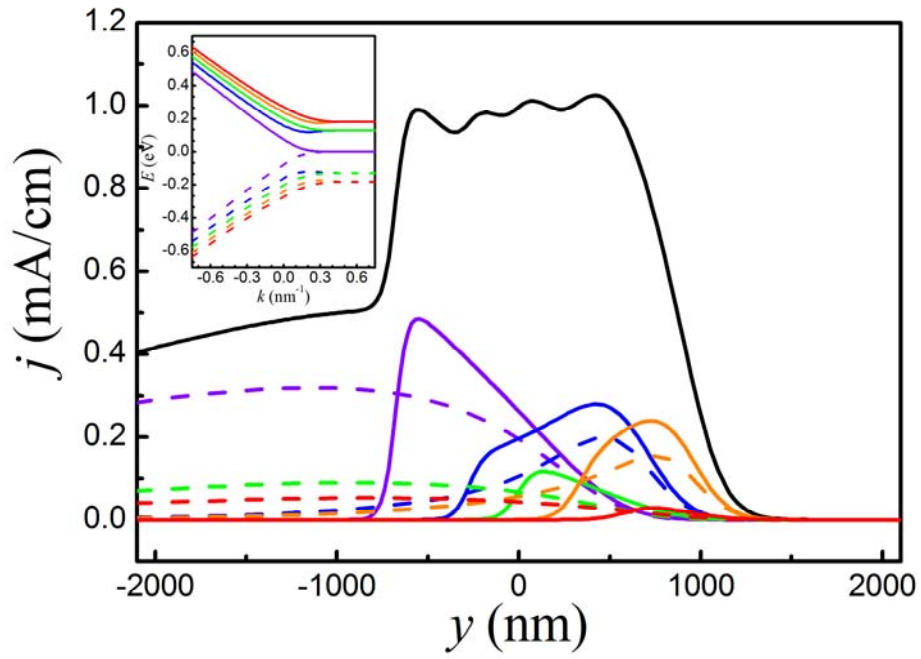


Fig.2 The y -directional current line density on the screen for $F_0 = 20\text{V}/\mu\text{m}$, $B = 15\text{Tesla}$, $T = 77\text{ Kelvin}$, and $\Delta = 0.2\text{ eV}$. Black solid curve is the total line density. Each colored curve is the partial line density of an individual Landau level as given in the inset in the same color.

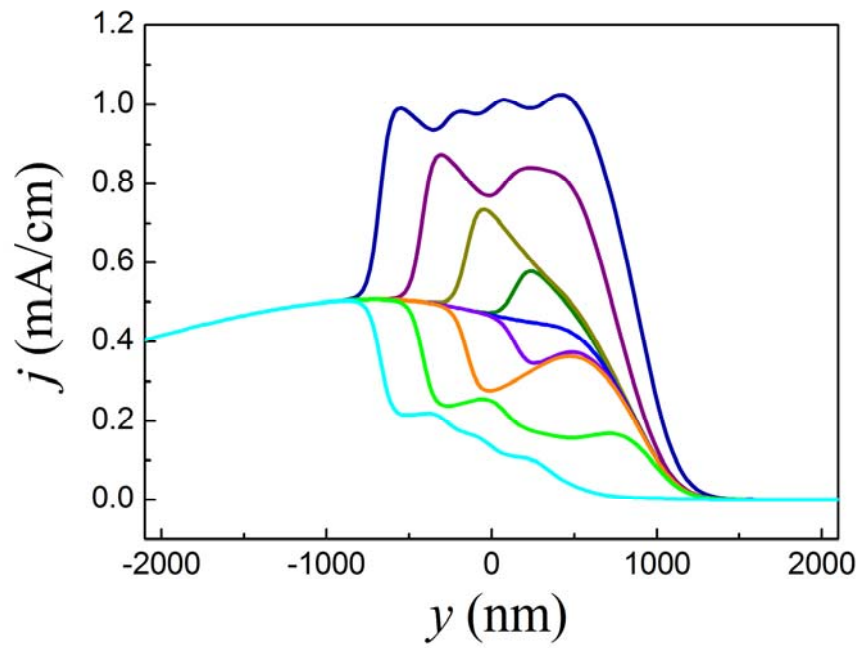


Fig.3 (color on line) The y -directional current line density on the screen for $F_0=20\text{V}/\mu\text{m}$, $B=15\text{Tesla}$, and $T = 77$ Kelvin. From the bottom to the top, the edge energy shifts are ranged from -0.2eV to 0.2eV , increasing with step 0.05eV

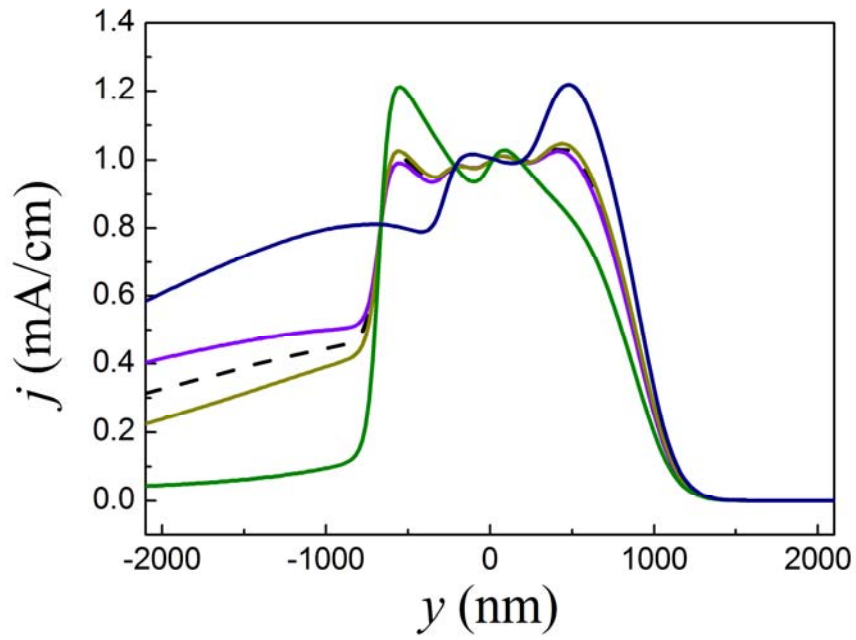


Fig.4 (color on line) The phase dependence of the line current density on the screen for $F_0 = 20 \text{ V}/\mu\text{m}$, $B = 15 \text{ Tesla}$, $T = 77 \text{ Kelvin}$, and $\Delta = 0.2 \text{ eV}$. The black dashed curve is the un-polarized density. The solid curves with their left wings from higher level to lower level are corresponding to phase shifts $-\pi/2, 0, \pi$, and $\pi/2$, respectively.